Compatibility of high-altitude aeromagnetic and satellite-altitude magnetic anomalies over Canada

GEOPHYSICS, VOL. 67, NO. 2 (MARCH-APRIL 2002); P. 546–554, 6 FIGS., 3 TABLES.
10.1190/1.1468615

Compatibility of high-altitude aeromagnetic and satellite-altitude magnetic anomalies over Canada

D. Ravat*, K. A. Whaler‡, M. Pilkington**, T. Sabaka§, and M. Purucker§

ABSTRACT

Results from equivalent-source distributions derived jointly from high-altitude (average 4 km) aeromagnetic and Magsat-derived (average 400 km) magnetic anomalies over Canada indicate that long-wavelength components (500–2500 km) in these fields are extremely compatible with one another (with a correlation coefficient of 0.95). The jointly estimated anomaly field at the earth's surface can be used as a long-wavelength adjustment surface for regional near-surface magnetic anomaly compilations and in assessing the performance of other downward-continuation techniques. Because near-surface anomalies are not available over all regions of the world, we compare the jointly estimated anomaly field to the results of two different downward-continuation techniques: the evaluation of anomalies at the earth's surface from spherical harmonic coefficients derived from satellite-altitude data and the use of downward-continuation methods based on harmonic splines. Numerical and visual comparisons of these downward-continued fields with the jointly estimated anomaly field from the equivalent-source method indicate they are well correlated and could provide a useful method of deriving long-wavelength leveling surfaces for regional and worldwide magnetic anomaly maps.

INTRODUCTION

Since the early days of isolating crustal signals from near-earth space-borne sensors (e.g., COSMOS, POGO, Magsat), numerous attempts have been made to verify the crustal component of satellite magnetic anomalies. Some of these attempts used both qualitative and quantitative comparisons of satellite data with upward-continued aeromagnetic data (Langel et al., 1980; von Frese et al., 1982; Won and Son, 1982; Schnetzler et al., 1985; Arkani-Hamed and Hinze, 1990) or downward-continued satellite data (Arkani-Hamed et al., 1985). The results of many of these studies implied that the correlation between the aeromagnetic and satellite anomalies was generally poor, but there were also significant similarities between the two data sets.

Arkani-Hamed et al. (1995) compared marine magnetic and satellite-altitude anomalies in the Atlantic Ocean; more recently, Pilkington and Roest (1996) compared high-altitude aeromagnetic data over Canada with the combined POGO and Magsat anomalies of Arkani-Hamed et al. (1994). Both of these studies, which utilized long tracks of near-surface data (as opposed to stitched-map compilations), found that many anomaly features were coincident on the near-surface and satellite-altitude maps and showed much better correspondence in many visual attributes of the anomalies than in any previous regional-scale comparisons between data sets. However, for the same features the amplitudes of the satellite anomalies were significantly smaller than the amplitudes of the upward-continued aeromagnetic maps.

In theory, upward continuation is a stable process; but, as we discuss later, inaccuracies in the long-wavelength components of the measured field at the surface can significantly affect the result—especially when the field is continued upward to satellite elevation.

While the response of many geologic sources of interest to exploration is merged in the satellite-altitude magnetic anomaly data, important advantages of the global coverage of these data are to establish long-wavelength base levels for continent-scale magnetic compilations and to potentially fill in gaps in the near-surface magnetic maps (Paterson, 1997). Long-wavelength anomaly components are also important in inferring the depth to the Curie isotherm from magnetic data (Blakely, 1995), a problem with definite implications for exploration geophysics. They are also important in understanding the sources of regional anomalies—the isolation of residual

Manuscript received by the Editor December 10, 1999; revised manuscript received July 30, 2001.
*Southern Illinois University at Carbondale, Department of Geology, MS 4324, Carbondale, Illinois 62901-4324. E-mail: ravat@geo.siu.edu.
‡Grant Institute, Department of Geology and Geophysics, West Mains Road, Edinburgh EH9 3JW, Scotland. E-mail: whaler@mail.glg.ed.ac.uk.
**Geological Survey of Canada, 615 Booth St., Ottawa, Ontario K1A 0E9, Canada. E-mail: mpilkington@nrcan.gc.ca.
§Raytheon-STX/Geodynamics Branch, Code 921, Goddard Space Flight Center, National Aeronautics & Space Administration, Greenbelt, Maryland 20771. E-mail: sabaka@geomag.gsfc.nasa.gov;-purucker@geomag.gsfc.nasa.gov.

and regional anomalies being critical in the interpretation of the data.

Both satellite-altitude and near-surface data have errors, and it is important to compare them using methods that can consider these errors. After a study of profiles extracted from the U.S. portion of the Decade of North American Geology project's aeromagnetic anomaly map of North America (DNAG aeromagnetic map) and independent data collected along long flight lines, Grauch (1993) suggestes that wavelengths >500 km and <170 km in the DNAG aeromagnetic map may be problematic, principally because of artifacts associated with datum shifts and survey height differences between the individual surveys. Since the two types of data themselves have artifacts and errors, complete agreement between them is unlikely when the aeromagnetic data set is upward continued to the altitude of satellite data. Therefore, we ask, "To what extent are the two anomaly data sets compatible with each other?" (We use the word compatible to imply a high level of similarity. In different applications, the acceptable level of significance of correlation or coherence can be somewhat different, for example, depending on the size and resolution of the survey, and cannot be quantified without a large number of model studies or examples. Our results are based on tests of five regional data sets. Until more experience is gained with the technique of this paper, we recommend using the word compatible to describe a high level of similarity.)

The question of compatibility can be addressed through joint inversion of the two data sets for an assumed distribution of sources such as equivalent sources suggested by Dampney (1969), applied in spherical coordinates by Mayhew (1979), von Frese et al. (1981), and Dyment and Arkani-Hamed (1998). If the same distribution of equivalent sources can reproduce (to a high level of correspondence) the potential fields over the same region at both aeromagnetic and satellite altitudes, then the data are compatible. If not, one or both must have errors, at least in certain wavelength ranges, making them incompatible. Because spatial data sets do not map all wavelengths with the same accuracy, it is also necessary to investigate and understand the extent to which each data set is valid in different wavebands. These are the questions addressed in this study.

We have also attempted to minimize many of the potential causes leading to disparities between the two data types. In particular, we have

1) used an aeromagnetic data set that inherently contains longer wavelengths than most aeromagnetic data (by virtue of having longer flight lines and using a main field model that spanned the time period of the surveys), thus minimizing leveling inaccuracies;
2) removed a degree 13 main field model from both data sets;
3) performed joint spherical-coordinate equivalent source inversions; and
4) used appropriate conversions of coordinate systems to represent data locations (aeromagnetic data are usually in geodetic coordinates, and satellite-derived data are in geocentric coordinates; an incorrect coordinate system causes shifts in latitude and differences in observation altitude).

Compatibility is evaluated at both altitudes (aeromagnetic and satellite) using quantitative comparison tools, e.g., the computation of spatial correlation coefficients; linear regression coefficients; and power, phase, and coherence spectra. Satellite-altitude magnetic anomalies are then continued downward to the level of aeromagnetic altitudes by means of the technique developed by Whaler (1994) and also by the usual spherical harmonic methods (Langel and Hinze, 1998). These maps are then compared against the jointly estimated anomaly maps at aeromagnetic altitude from the equivalent-source inversion to understand the effectiveness of the downward-continuation techniques in producing low-altitude base maps for compiling near-surface magnetic surveys.

ANOMALY DATA SETS

Aeromagnetic data

For the comparisons intended in this study, an aeromagnetic data set must have as accurate as possible long-wavelength (>500 km) components because those are the wavelengths at which the available satellite-altitude anomalies have meaningful information. We used high-altitude (3–6 km), total-intensity magnetic field data collected over Canada by the former Earth Physics Branch (EPB) of the Canadian Department of Energy, Mines, and Resources from 1969 to 1976 (Haines, 1983; Pilkington and Roest, 1996). The data were collected with long flight lines, commonly >2000 km long, with a line spacing varying from 30 to 75 km. Although no specific external field corrections were made, data were accepted only if the magnetic field measured at magnetic observatories on either side of the measurement location in the geomagnetic latitude was within 100 nT of its quiet level for more than 3 hours (Haines, 1983; Pilkington and Roest, 1996). The resulting anomaly map is shown in Figure 1.

To achieve the long-wavelength veracity in the aeromagnetic anomaly compilations, it is necessary to remove a core field model appropriate for the data acquisition period. Of all the available core field models, the GSFC/CU (12/96) model (Langel et al., 1996; Sabaka et al., 2000) was used because it extends to spherical harmonic degree and order 13 (similar to those from satellite data) and spans the period from mid-1960s to 1980 (i.e., covers the time period of the EPB surveys).

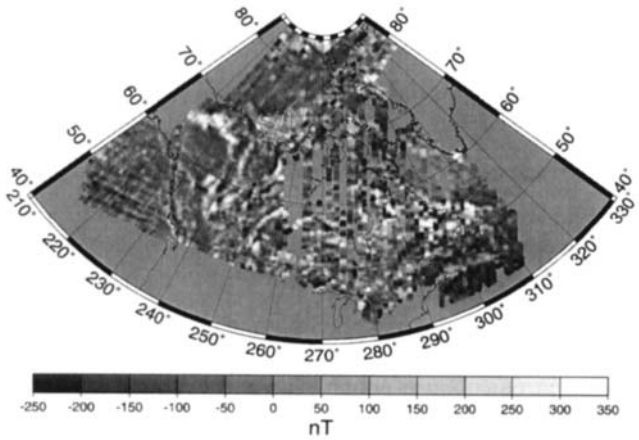

FIG. 1. The gridded (0.2° spacing) image of the total-intensity EPB aeromagnetic anomaly data with reference to GSFC/CU 12/96 main magnetic field model.

Preparation of aeromagnetic data

Analytical continuation using the flat-earth rectangular coordinate approximation causes inaccuracies because of the actual sphericity of the earth and the large upward-continuation height (up to about 16% error based on the formula of Vints et al., 1970). Therefore, a spherical coordinate equivalent-source inversion (Mayhew, 1979; von Frese et al., 1981; Dyment and Arkani-Hamed, 1998) was chosen for comparison purposes.

An inversion with the number of dipoles required to represent the whole EPB data set (at roughly 5–10-km dipole spacing) would need significant computer resources. One way to reduce the number of dipoles without compromising the integrity of the process is to filter out short-wavelength anomalies which are attenuated below the noise level of the satellite-altitude data. We verified that anomalies $\leq$500 km wavelength in the EPB data, when continued upward to 400 km, result in amplitudes <1 nT, which is lower than the error level in satellite anomaly maps. Thus, we filtered out wavelengths <500 km from the aeromagnetic data (the low-pass filter was tapered linearly from 400 to 600 km). We reached the same conclusion regarding the wavelength cutoff appropriate at 400 km altitude by using the anomaly amplitude/wavelength information from the EPB data in conjunction with the theoretical rectangular coordinate upward-continuation relationship (Dean, 1958), $T_{up} = T_0 e^{-(2\pi/\lambda)z}$, where T_0 and T_{up} are the amplitudes of the anomaly wavelength λ (full wavelength) at the original and the upward-continued altitudes and z is the upward-continuation height.

The low-pass filtered field values were averaged over 1° latitude/longitude intervals, where data were available, giving 3402 values (Figure 2a). The resulting data set contained wavelengths >500 km and could be represented well with an equal-area equivalent-dipole spacing of about 100 km. The number of such dipoles that cover the area between 40°N and 87°N latitude and 150°W and 30°W longitude is 2566.

Satellite magnetic anomaly map

Of all the satellite altitude anomaly maps we tested using the method described in the next section (Cain et al., 1990; Langel, 1990; Ravat et al., 1995; Alsdorf et al., 1998), the Magsat magnetic anomaly map based on the model of Cain et al. (1990) (Figure 2b) was most similar to the aeromagnetic map in all numerical comparisons. This map comprises scalar values computed from spherical harmonic coefficients of degrees 14 to 49 at 400 km.

JOINT EQUIVALENT-SOURCE INVERSION AND COMPARISONS

The efficacy of equivalent-source inversion is dependent on the source spacing, the source depth, the proximity to the geomagnetic equator (von Frese et al., 1988), and, for joint inversions, the weighting of the satellite and aeromagnetic anomaly values. In this study, instability in the inversion near the geomagnetic equator was not an issue.

Best-fit equivalent source depths of the combined EPB aeromagnetic and satellite data

The optimum source depth was determined by examining the misfit to each of the data sets from inversions with equivalent sources at different depths. Remember that the best-fitting equivalent dipole/point mass approximating a nonspherical volume of material with uniform physical properties will always be below the centroid of the material (see the model study in Ravat et al., 1991). The satellite and the EPB aeromagnetic data sets show minima between the observed and computed anomalies at about 100- and 200-km depths, respectively (Table 1); we chose 100 km as the source depth for the final inversions. In this case, the equivalent sources are only a mathematical convenience to represent the field; it is possible to convert their dipole moments into bulk crustal volume susceptibilities using the procedure given by Ravat et al. (1991) if the thickness of the magnetic crust is known and the remanent magnetization is negligible.

Inverse problem and weighting of data sets

We form the following system of equations represented by matrices

$$\mathbf{A}\,\mathbf{x} = \mathbf{b}, \tag{1}$$

where $\mathbf{A}$ is the matrix of source-to-observation distance functions (Langel and Hinze, 1998, chapter 5), $\mathbf{x}$ is the vector

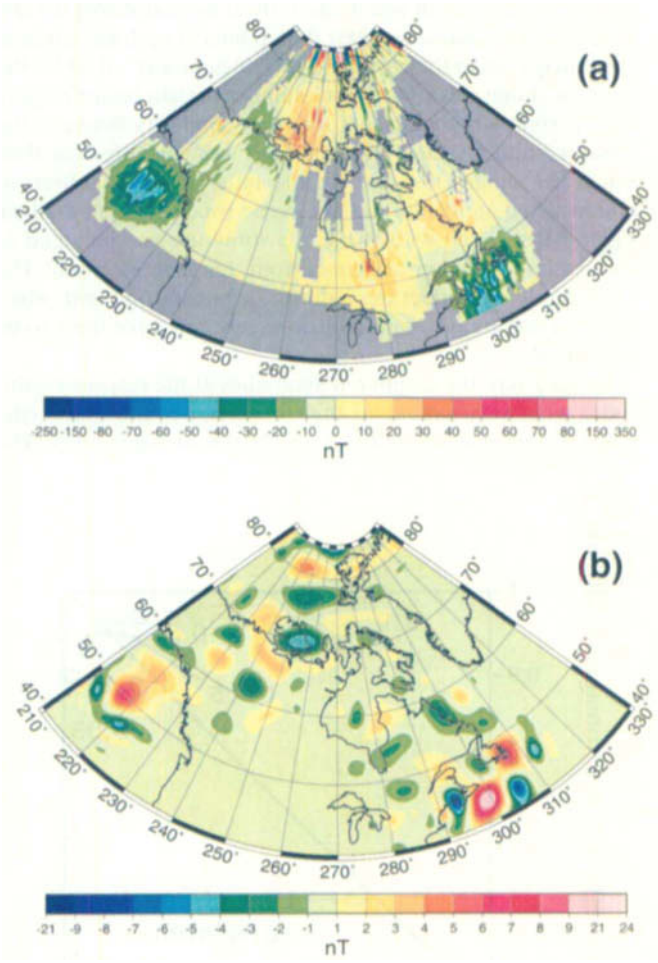

FIG. 2. The observed anomaly maps. (a) Long-wavelength (>500 km) EPB aeromagnetic anomalies averaged at 1° spacing. (b) Scalar anomalies computed from Cain et al.'s (1990) m102389 field model (degrees 14 to 49, both inclusive).

of dipole moments or susceptibilities, and **b** is the vector of observations. We calculate a weighted least-squares solution (Menke, 1989),

$$\mathbf{x} = (\mathbf{A}^T\mathbf{w}^T\mathbf{w}\,\mathbf{A})^{-1}\mathbf{A}^T\mathbf{w}^T\mathbf{w}\,\mathbf{b}, \qquad (2)$$

where the elements of the weight matrix **w** are determined using the procedure given below.

There are two reasons to weight the aeromagnetic and satellite data differently. One is that the anomalies in the two data sets have different amplitudes (±350 nT in aeromagnetic anomalies versus ±25 nT in satellite-altitude anomalies) and uncertainties (from positioning errors, ionospheric contamination, instrumental noise, etc.). Based on dawn and dusk differences from the Magsat data in the Arctic region, we estimate these errors to be on the order of 1 to 3 nT. The errors in the EPB aeromagnetic data are on the order of 50 nT (Haines, 1983).

Another reason for weighting the data differently is the role that the matrix of the source-to-observation distance function [**A** in Equation (1)] plays during the inversion. Because of the inverse distance function, the matrix elements corresponding to the satellite data are very small in comparison with the elements corresponding to the aeromagnetic data. The satellite data therefore have negligible influence in an unweighted joint inversion. It is important to note that each of the data sets can be matched independently without any weighting. The data resolution matrix (Menke, 1989), also known as the information density matrix, is a data-by-data matrix describing how well the predicted data match the observations, and it is the identity matrix for a perfect fit to the data. Since it is rather large, we calculated it only over a 10° × 10° subregion. Over this subregion, the average of the diagonal elements associated with aeromagnetic data locations was 0.76, whereas the corresponding average for the satellite data locations was only 0.02. The calculations indicated that, to achieve equality in the joint inversion, the satellite data must be weighted more than the aeromagnetic data.

The exact weighting required for the least-squares problem is difficult to gauge using the 10° × 10° data resolution matrix. Thus, we adopted the following approach to find the relative weighting for the two data sets in the inversion. The weighting was decided on the basis of how well differently weighted inversions were able to reproduce the anomalies at both aeromagnetic and satellite altitudes. Spatial correlation coefficients between the observed data and the anomalies computed from the set of dipoles provided an objective criterion. Inversions were performed with various weightings: optimum weights could be relatively easily chosen (in this case, because the two data sets are highly compatible) at a point where the correlation coefficients at satellite and aeromagnetic altitudes were roughly equal (in each of these sets the number of values and their distribution are similar; see Figure 3).

When the data sets are incompatible, which was the case in a comparison study performed over the Urals portion of the former Soviet Union aeromagnetic map, the correlation coefficients were not high simultaneously at both altitudes for any weight. For example, with 961 data points at each elevation in these maps, when the correlation coefficient was >0.90 for the data set at one elevation (small number of data points require high correlation coefficients for close similarity between the observed and inverted anomalies), it was <0.50 for the data set at the other elevation (in the latter case, the observed and inverted anomalies did not even visually appear similar). Figures associated with the Urals study are not included to avoid a large number of figures from this separate study. The Urals study is in effect the null test demonstrating that, when the data sets are incompatible, no weight can force them to be compatible.

In our study, the computed anomalies at the respective altitudes were very similar to their observed counterparts (the map at aeromagnetic altitude is shown in Figure 6a). The

Table 1. Depth of equivalent-source dipoles was based on best fit to observed satellite and low-pass EPB aeromagnetic data and computed anomalies from the jointly inverted data sets by placing dipoles at various depths. The best fit depths are highlighted.

Depth below mean earth radius (km)	Sum of squared difference of observed & computed EPB data (nT^2)	Sum of squared difference of observed & computed satellite data (nT^2)
30	3 283 038	174 748
50	3 797 670	259 002
70	2 730 244	259 457
100	1 045 937	**94 400**
200	**734 971**	146 782
300	899 532	215 089

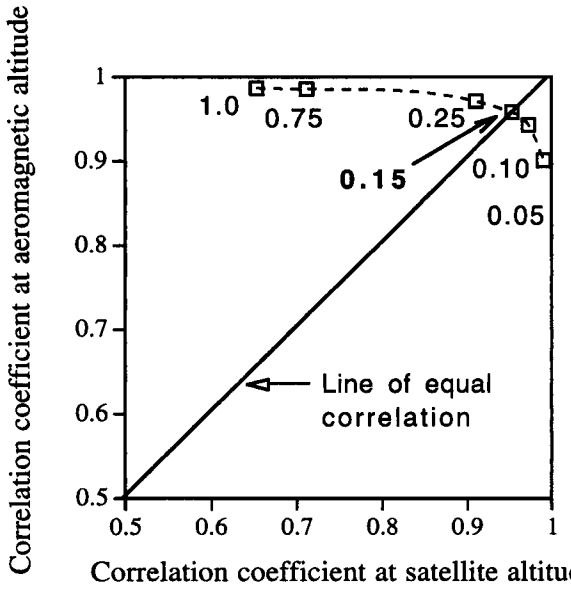

FIG. 3. A trade-off curve showing the correlation coefficients between the observed anomalies and the anomalies computed from the joint equivalent-source inversion of data in Figure 2. Points of the curve represent the relative amount of weighting applied to the EPB aeromagnetic anomalies, 1 nT^{-1} being the weighting for the satellite anomalies. Low weighting for the aeromagnetic data is required for both satellite and aeromagnetic data exercise to roughly equal influence in this problem (see the text for details). Aeromagnetic data weights of 0.15 nT^{-1} were chosen for subsequent calculations.

difference maps between the observed and computed anomalies (Figure 4) indicate that, over most of the region, the differences at aeromagnetic and satellite altitude are on the order of ±20 and ±1 nT, respectively—less than the estimated uncertainties. Because the satellite data are collected and processed more homogeneously than aeromagnetic data, the limited areas of larger differences indicate that problems may exist in or near edges of some of the aeromagnetic surveys. The results from the quantitative comparisons of the EPB aeromagnetic data and the Magsat magnetic anomaly data of Cain et al. (1990) are presented in Table 2. The slopes (from a linear regression of observed and inverted anomalies) and correlation coefficients close to unity indicate a similarity of their amplitudes and a high degree of association between the two data sets, respectively. The intercepts (from the linear regression) are all very small with respect to the respective data ranges, indicating that no significant base-level differences exist between the data sets.

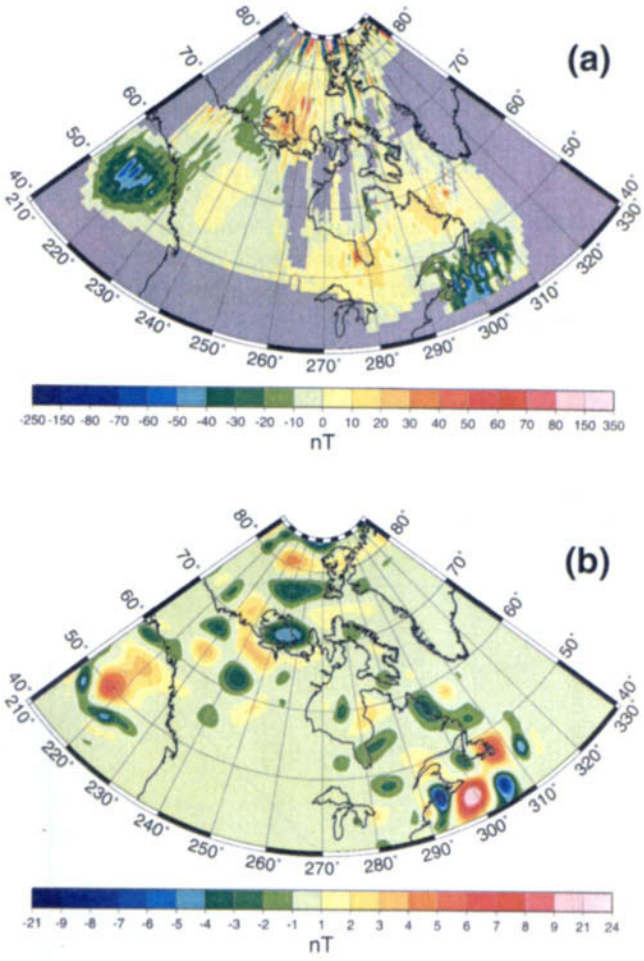

FIG. 4. Difference maps between the observed anomalies (Figure 2) and the anomalies computed from the inversion: (a) at aeromagnetic altitude (3–6 km), (b) at satellite altitude (400 km).

Wavenumber-domain comparisons between the satellite and aeromagnetic anomalies

The above tests yield only global estimates of the correspondence between the data sets. Estimates based on the comparisons of wavenumber spectra yield information related to the individual wavenumber components. These techniques include coherence and amplitude/phase spectra and wavenumber-domain correlation coefficients (cosine of the phase difference at each wavenumber) (Kanasewich, 1981; Arkani-Hamed and Strangway, 1986; Alsdorf et al., 1994). The coherence measures the amount of association between two data sets in a band of wavenumbers about a central wavenumber (Kanasewich, 1981). The coherence and power between the observed anomalies [Cain et al. (1990) model and the EPB aeromagnetic anomalies] and the anomalies computed from the joint inversion are shown in Figures 5a and 5b, respectively. At the relevant wavenumbers, the association is strong for the comparisons at both altitudes, as indicated by coherence values of >0.80. The coherence at satellite altitude is not high at wavelengths <600 km because the highest spherical harmonic degree of the model we used here is 49, which has a corresponding rms wavelength (λ_{rms}) of 645 km using the formula

$$\sqrt{\frac{2 \cdot \text{area of sphere}}{n(n+1)}}$$

derived by Coerte Voorhies (personal communication, 1998), where n is the highest degree of the model. Note that the drop in coherence is accompanied by an increased phase difference (Figure 5c). The coherence is high at aeromagnetic altitudes for all wavelengths considered here (i.e., 500–2500 km).

ESTIMATING ANOMALIES FROM SATELLITE-ALTITUDE DATA AT THE EARTH'S SURFACE

The jointly estimated long-wavelength aeromagnetic anomalies derived from optimization of information in both aeromagnetic and satellite-altitude magnetic data are illustrated in Figure 6a. To this result, we can easily add the short-wavelength anomalies (<500 km wavelength) to produce a Magsat-leveled aeromagnetic anomaly map, as illustrated with the example over the continental U.S. by Ravat and Purucker (1999). We

Table 2. A comparison of correlation coefficient, slope, and intercept between the observed anomalies and the anomalies computed from a joint inversion of a single set of equivalent dipoles. The weighting on EPB anomalies is 0.15 nT^{-1}. The weighting for satellite data is 1.0 nT^{-1}.

Correlation coefficient for aeromagnetic comparison	Slope for aeromagnetic comparison	Intercept for aeromagnetic comparison (nT)	Correlation coefficient for satellite comparison	Slope for satellite comparison	Intercept for satellite comparison (nT)
0.96	0.93	2.07	0.95	1.01	−0.08

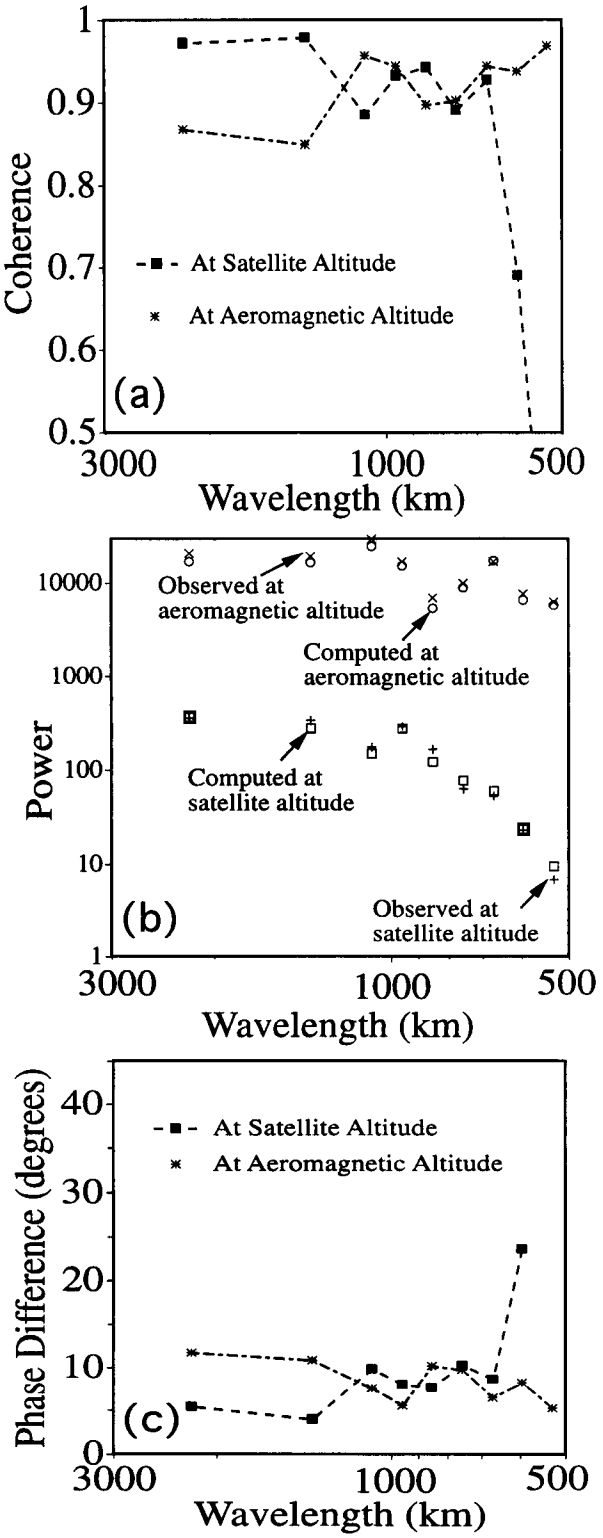

FIG. 5. (a) Coherence, (b) power, and (c) phase difference between observed and computed anomalies from the joint inversion at aeromagnetic and satellite altitudes. The satellite data for this computation were from Cain et al.'s (1990) m102389 model. The fields at both altitudes compare very well.

do not show the resulting map here because the leveled map is visually indistinguishable from Figure 1; however, the change between the original and the leveled maps can be accurately judged from Figure 4a.

We believe that the estimation of the long-wavelength field in Figure 6a is the best that can be achieved in the present circumstances, but it requires data at both altitudes over roughly the same locations on the earth. However, near-surface anomalies are not available over all regions; therefore, we would like to compare the anomalies of Figure 6a with the results of downward continuation of satellite anomalies from other techniques.

Six different downward-continued fields were examined (the last two use the EPB data as well) [we use Cain et al. (1990) nomenclature to distinguish their anomaly fields]:

1) the anomaly calculation at aeromagnetic level from Cain et al.'s degree 49 spherical harmonic field model (m102389);
2) the same from Cain et al.'s degree 60 spherical harmonic field model (m102189) (wavelengths from 525 to 2500 km) (Figure 6b);
3) depleted-basis harmonic spline downward continuation from Cain et al.'s degree 49 spherical harmonic field model;
4) same as #3 from Cain et al.'s degree 60 spherical harmonic field model (Figure 6c);
5) same as #3 but also including the EPB data; and
6) same as #4, including the EPB data (Figure 6d).

The results are listed in Table 3 in the form of correlation coefficients and slopes. Cain et al. (1990) originally thought that high spherical harmonic degrees (50–60) in their m102189 model were contaminated by noise. However, a comparison of the slopes (amplitudes) in Table 3 shows that the anomalies from these high degrees are probably meaningful.

The first two anomaly fields are the evaluations of the spherical harmonic coefficients of Cain et al. (1990) at aeromagnetic altitude. The anomalies in Figures 6a and 6b are similar in their overall appearance, although some of the anomalies appear stronger in one or the other data set (e.g., anomalies at 52°N, 270°E and 58°N, 305°E are stronger in Figure 6b, whereas the anomaly at 70°N, 295°E and the anomalies near 65°N, 250°E are stronger in Figure 6a). Also, anomalies in Figure 6b appear to be more north–south trending. The amplitude range of the anomalies based on m102189 coefficients (Figure 6b) is very similar to the result shown in Figure 6a, and the correlation coefficient indicates significant correlation between the two data sets (Table 3). In fact, the probability that random samples would result in any of the correlation coefficients in Table 3 is much less than 0.01% (Bevington, 1969). For the correlation coefficients to be meaningful, the results imply that the standard deviation of the errors in the data are approximately 40 nT (e.g., Press et al., 1992). This is reasonable, considering the 50-nT error estimated a priori for the EPB surveys (Haines, 1983).

For the last four of the anomaly fields, we used the method of depleted basis harmonic splines (Parker and Shure, 1982; Shure et al., 1982) to downward continue, using satellite data alone and jointly modeling the satellite and EPB data (Whaler, 1994; Langel and Whaler, 1996). The method is described in detail in Langel and Hinze (1998, chapter 5). The distribution of basis points, the parameters through which the downward

continued field was expressed and whose spacing governs the resolution of the model, was concentrated over Canada (with 3° spacing over the map areas shown in Figure 6 and resulting in 1724 parameters). A much finer spacing would be required to represent the detail of the aeromagnetic anomalies; hence, it is not computationally practical for representing short wavelengths in regional compilations. As with any inversion, a range of models can be produced by varying the fit to the data through

Table 3. Comparison of the jointly-estimated long-wavelength anomalies at aeromagnetic altitude (Figure 6a) with various downward-continued data sets.

Downward-continuation anomaly field/method	Number of points	Correlation coefficient	Slope
m102389[a]; spherical harmonic expansion	3636	0.52	0.53
m102189[b]; spherical harmonic expansion	3636	0.54	0.84
m102389[c]; Whaler (1994)	85 671	0.52	0.65
m102189[d]; Whaler (1994)	85 671	0.53	1.09
m102389 and EPB[e]; Langel and Whaler (1996)	85 671	0.65	0.93
m102189 and EPB[f]; Langel and Whaler (1996)	85 671	0.67	1.02

[a]Scalar anomalies computed from m102389 model of Cain et al. (1990), degrees 14–49.
[b]Scalar anomalies computed from m102189 model of Cain et al. (1990), degrees 14–60 (Figure 6b).
[c]Harmonic spline downward continuation of m102389 model, degrees 14–49.
[d]Harmonic spline downward continuation of m102189 model, degrees 14–60 (Figure 6c).
[e]Joint harmonic spline modeling of m102389 model, degrees 14–49, and the EPB data.
[f]Joint harmonic spline modeling of m102189 model, degrees 14–60, and the EPB data (Figure 6d).

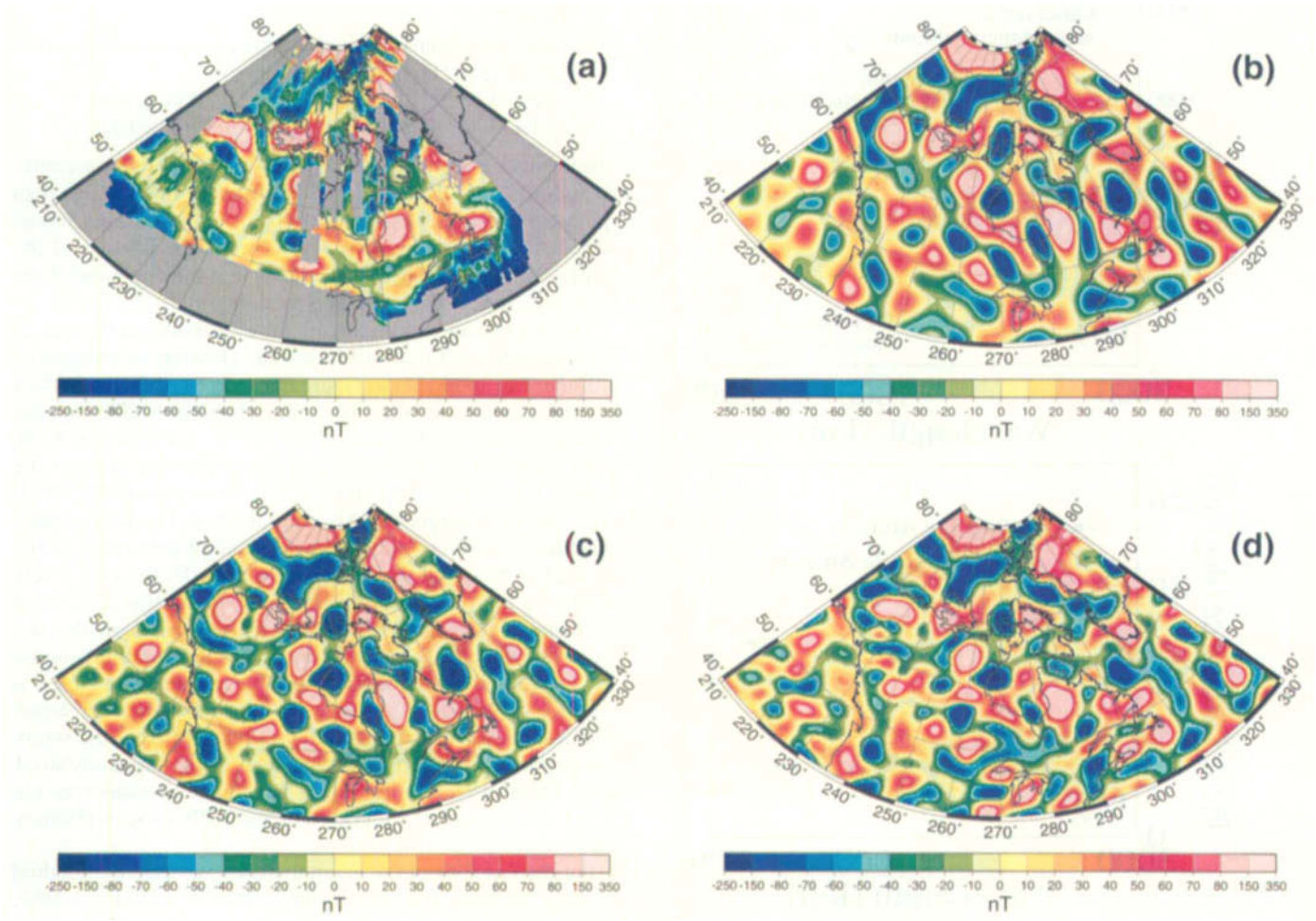

FIG. 6. (a) The jointly inverted anomaly field at aeromagnetic altitude (3–6 km) with the following three downward-continued scalar anomaly fields. (b) The anomaly calculation at aeromagnetic level from Cain et al.'s (1990) m102189 spherical harmonic model (degrees 14–60). (c) Harmonic spline downward continuation of satellite altitude anomalies from the m102189 spherical harmonic model (degrees 14–60). (d) Joint harmonic spline downward estimation of the anomalies in (c) and the EPB data where available. See Table 3 for numerical comparisons.

a damping parameter, and we chose our preferred models without reference to their agreement with other maps. The result of the downward continuation of anomalies calculated from Cain et al.'s m102189 spherical harmonic model from 400 to 4 km altitude with this method is shown in Figure 6c. This map is once again correlated to the map in Figure 6a at a statistically meaningful level (Table 3).

For the joint estimation of Cain et al.'s m102189 spherical harmonic field and the scalar EPB data at aeromagnetic altitude, we used the technique of Langel and Whaler (1996). Because of the separation of the basis points, some of the resolution of the EPB data has been lost, but this technique also allows comparison of the longer wavelength component of the EPB data with the satellite model. Our preferred joint model (by choice of the damping parameter) in Figure 6d shows long-wavelength features in common with the satellite-only model of Figure 6c, but some smaller-scale features superimposed arise from inclusion of the EPB data. Downward-continued anomaly fields are able to reproduce the overall range of anomaly amplitudes correctly (Table 3), and many long-wavelength features between the maps compare sufficiently well. While these correlation coefficients and visual comparisons imply that uncertainties have been partially mapped in the downward-continued anomalies, the similarities are also many. Thus, it appears that the downward-continued field from the satellite-altitude magnetic anomaly data may be used to define the long-wavelength features of the regional and world magnetic anomaly maps (Paterson, 1997).

CONCLUSION

Using appropriately weighted joint inversion of aeromagnetic (EPB: Haines, 1983; Pilkington and Roest, 1996) and satellite-altitude (Magsat: Cain et al., 1990) anomaly fields, we have shown that the two fields over Canada are highly compatible (correlation coefficients >0.95, slopes ≈ 1, coherence >0.85) over the wavelength range from about 500 to 2500 km (at the EPB data altitude). The high level of compatibility between these fields allows determination of the optimum long-wavelength magnetic anomaly field at aeromagnetic altitude. We can combine this field with the short-wavelength (<500 km) magnetic anomalies to recreate the entire spectrum of magnetic anomalies of the two data sets. Similar high correlations between the long-wavelength aeromagnetic and satellite anomaly fields were also observed over the continental U.S. (Ravat and Purucker, 1999; Wang et al., 2000) and portions of Antarctica (von Frese et al., 1999). It is also important to appreciate that when data sets are not compatible, high correlation coefficients cannot be obtained simultaneously at both levels with any weighting (e.g., as in the Urals study). These comparisons indicate that the use of satellite-altitude magnetic anomalies would prove advantageous when adjusting the long wavelengths in regional aeromagnetic compilations and for filling gaps in the aeromagnetic coverage in these compilations. When aeromagnetic data become available in the regions of gaps, those areas can be treated similarly as the rest of the compilation.

Because aeromagnetic data are not available everywhere, downward continuation of satellite anomalies alone is examined using two different methods: one from the evaluation of spherical harmonic coefficients computed using satellite-altitude data (Cain et al., 1990) and the other from harmonic spline downward continuation. Based on statistically meaningful correlation coefficients and values of regression parameters, both downward-continuation techniques appear to map the field adequately. Statistical parameters also indicate that the performance of the latter method, with the inclusion of aeromagnetic data, is improved as one might expect.

With future lower-altitude magnetic satellite missions, such as the German CHAMP mission, which is expected to measure the field at 250 km altitude for some time, the joint estimation could include wavelengths as short as 300 km or lower. Reliable anomalies at these wavelengths would be extremely useful for interpreting magnetic data, especially in addressing important geodynamic and exploration issues related to lower crustal/upper mantle magnetizations and mapping of the Curie isotherm.

ACKNOWLEDGMENTS

We thank Bob Parker for advice on multitaper spectral estimations. We also thank Coerte Voorhies, Rick Blakely, Tom Hildenbrand, and Herb Frey for discussions and helpful suggestions. We thank John Peirce, three anonymous reviewers, and the associate editor (Afif Saad) for useful reviews. We are grateful to Joe Cain for the use of his Magsat field models in this study. Doug Alsdorf also provided his Arctic map for comparison. Dave Bailey did some of the downward-continuation calculations. Bingzhu Wang performed the Urals study. Processing and plotting was simplified with the use of GMT software (Wessel and Smith, 1995). The majority of the funding was provided by NASA; we are grateful for this generous support. For their hospitality, D.R. thanks members of the Geodynamics Branch at Goddard Space Flight Center (NASA). We would like to dedicate this paper to the memory of Bob Langel, who was extremely interested in the results of this study and who made many useful suggestions during the project.

REFERENCES

Alsdorf, D., Taylor, P., von Frese, R., Langel, R., and Frawley, J., 1998, Arctic and Asia lithospheric satellite magnetic anomalies: Phys. Earth Planet. Internat., **108**, 81–99.

Alsdorf, D. E., von Frese, R. R. B., Arkani-Hamed, J., and Noltimier, H. C., 1994, Separation of lithospheric, external and core components of the south polar geomagnetic field at satellite altitudes: J. Geophys. Res., **99**, 4655–4668.

Arkani-Hamed, J., and Hinze, W. J., 1990, Limitations of the long-wavelength components of the North American magnetic anomaly map: Geophysics, **55**, 1577–1588.

Arkani-Hamed, J., and Strangway, D. W., 1986, Magnetic susceptibility anomalies of lithosphere beneath eastern Europe and the Middle East: Geophysics, **51**, 1711–1724.

Arkani-Hamed, J., Langel, R. A., and Purucker, M., 1994, Scalar magnetic anomaly maps of earth derived from POGO and Magsat data: J. Geophys. Res., **99**, 24 075–24 090.

Arkani-Hamed, J., Strangway, D. W., Teskey, D. J., and Hood, P., 1985, Comparison of Magsat and low-level aeromagnetic data over the Canadian Shield: Implications for GRM: Can. J. Earth Sci., **22**, 1241–1247.

Arkani-Hamed, J., Verhoef, J., Roest, W., and Macnab, R., 1995, The intermediate-wavelength magnetic anomaly maps of the north Atlantic Ocean derived from satellite and shipborne data: Geophys. J. Internat., **123**, 727–743.

Bevington, P. R., 1969, Data reduction and error analysis for the physical sciences: McGraw-Hill Book Co.

Blakely, R. J., 1995, Potential theory in gravity and magnetic applications: Cambridge Univ. Press.

Cain, J. C., Holter, W., and Sandee, D., 1990, Numerical experiments in geomagnetic modeling: J. Geomag. Geoelectr., **42**, 973–987.

Dampney, C. N. G., 1969, The equivalent source technique: Geophysics, **45**, 39–53.
Dean, W. C., 1958, Frequency analysis for gravity and magnetic interpretation: Geophysics, **23**, 97–127.
Dyment, J., and Arkani-Hamed, J., 1998, Equivalent source magnetic dipoles revisited: Geophys. Res. Lett., **25**, 2003–2006.
Grauch, V. J. S., 1993, Limitations on digital filtering of the DNAG magnetic data set for the conterminous U. S.: Geophysics, **58**, 1281–1296.
Haines, G. V., 1983, E.P. B. aeromagnetic data (1953–1976): Aeromagnetic Data Workshop, Nat'l. Oceanic and Atmos. Admin. (NOAA), Proceedings, 5–19.
Kanasewich, E. R., 1981, Time sequence analysis in geophysics, 3rd ed.: Univ. Alberta Press.
Langel, R. A., 1990, Global magnetic anomaly maps derived from POGO spacecraft data: Phys. Earth Planet. Interiors., **62**, 208–230.
Langel, R. A., and Hinze, W. J., 1998, The magnetic field of the earth's lithosphere: The satellite perspective: Cambridge Univ. Press.
Langel, R. A., and Whaler, K. A., 1996, Maps of the magnetic anomaly field at earth's surface from scalar satellite data: Geophys. Res. Lett., **23**, 41–44.
Langel, R. A., Coles, R. L., and Mayhew, M. A., 1980, Comparisons of magnetic anomalies of lithospheric origin measured by satellite and airborne magnetometers over western Canada: Can. J. Earth Sci., **17**, 876–887.
Langel, R. A., Sabaka, T. J., Baldwin, R. T., and Conrad, J. A., 1996, The near-earth magnetic field from magnetospheric and quiet-day ionospheric sources and how it is modeled: Phys. Earth Planet. Internat., **98**, 235–267.
Mayhew, M. A., 1979, Inversion of satellite magnetic anomaly data: J. Geophys., **45**, 119–128.
Menke, W., 1989, Geophysical data analysis: Discrete inverse theory: Academic Press Inc.
Parker, R. L., and Shure, L., 1982, Efficient modeling of the earth's magnetic field with harmonic splines: Geophys. Res. Lett., **9**, 812–815.
Paterson, N. R., 1997, Giving new life to old data: 50 years of airborne geophysics on view: Workshop on Airborne Geophysics, Assn. Expl. Geophys. (India), Proceedings, 85–92.
Pilkington, M., and Roest, W. R., 1996, An assessment of long-wavelength magnetic anomalies over Canada: Can. J. Earth Sci., **33**, 12–23.
Press, W. H., Teukolsky, S. A., Vetterling, W. T., and Flannery, B. P., 1992, Numerical recipes in Fortran, 2nd ed.: Cambridge Univ. Press.
Ravat, D., and Purucker, M., 1999, The future of satellite magnetic anomaly studies is bright!: The Leading Edge, **18**, 326–329.
Ravat, D. N., Hinze, W. J., and von Frese, R. R. B., 1991, Lithospheric magnetic property contrasts within the South American plate derived from damped least-squares inversion of satellite magnetic data: Tectonophysics, **192**, 159–168.
Ravat, D., Langel, R. A., Purucker, M., Arkani-Hamed, J., and Alsdorf, D. E., 1995, Global vector and scalar Magsat magnetic anomaly maps: J. Geophys. Res., **100**, 20111–20136.
Sabaka, T. J., Olson, N., and Langel, R. A., 2000, A comprehensive model of the near-earth magnetic field: Phase 3: NASA/TM-2000-209894.
Schnetzler, C. C., Taylor, P. T., Langel, R. A., Hinze, W. J., and Phillips, J. D., 1985, Comparison between the recent U.S. composite magnetic anomaly map and Magsat anomaly data: J. Geophys. Res., **90**, 2543–2548.
Shure, L., Parker, R. L., and Backus, G. E., 1982, Harmonic splines for geomagnetic modelling: Phys. Earth and Planet. Internat., **28**, 215–229.
Vints, B. D., Pochtarev, V. I., and Rakhmatulin, R. Sh., 1970, Method of computing the geomagnetic field upward in near-earth space: Geomag. and Aeronomy, **10**, 90–98.
von Frese, R. R. B., Hinze, W. J., and Braile, L. W., 1981, Spherical earth gravity and magnetic analysis by equivalent point source inversion: Earth and Planet. Sci. Lett., **53**, 69–83.
von Frese, R. R. B., Hinze, W. J., Sexton, J. L., and Braile, L. W., 1982, Verification of the crustal component in satellite magnetic data: Geophys. Res. Lett., **9**, 293–295.
von Frese, R. R. B., Kim, H. R., Kim, J. W., Taylor, P. T., Purucker, M. E., Alsdorf, D. E., and Raymond, C. A., 1999, Satellite magnetic anomalies of the Antarctic crust: Annali Di Geofisica, **42**, 309–326.
von Frese, R. R. B., Ravat, D. N., Hinze, W. J., and McGue, C. A., 1988, Improved inversion of geopotential field anomalies for lithospheric investigations: Geophysics, **53**, 375–385.
Wang, B., Ravat, D., Sabaka, T., and Hildenbrand, T., 2000, Long-wavelength magnetic field for the conterminous U.S. from project magnet and Magsat data: EOS Trans. Amer. Geophys. U., **81**, No. 48, F355.
Wessel, P., and Smith, W. H. F., 1995, New version of the Generic Mapping Tools released: EOS Trans. Amer. Geophys. U., **76**, 329.
Whaler, K. A., 1994, Downward continuation of Magsat lithospheric anomalies to the earth's surface: Geophys. J. Internat., **116**, 267–278.
Won, I. J., and Son, K. H., 1982, A preliminary comparison of the Magsat data and aeromagnetic data in the continental U.S.: Geophys. Res. Lett., **9**, 296–298.